

In situ fluorescence imaging of organs through compact scanning head for confocal laser microscopy

Taisuke Ota

Kyoto Prefectural University of Medicine
Department of Pathology and Cell Regulation
Kawaramachi-Hirokoji, Kamigyo-ku
Kyoto 602-8566, Japan

Hiroya Fukuyama

Yasushige Ishihara

Olympus Corporation
2951 Ishikawa-cho, Hachioji-shi
Tokyo 192-8507, Japan

Hideo Tanaka

Tetsuro Takamatsu

Kyoto Prefectural University of Medicine
Department of Pathology and Cell Regulation
Kawaramachi-Hirokoji, Kamigyo-ku
Kyoto 602-8566, Japan
E-mail: ttakam@koto.kpu-m.ac.jp

Abstract. We develop a compact scanning head for use in laser confocal fluorescence microscopy for *in situ* fluorescence imaging of organs. The head, cylindrical in shape, has 3.5 mm diameter and 30 mm length, and is thus small enough to operate in a living rat heart. The lateral and axial resolutions, defined as full widths at half maximum (FWHM) of a point spread function (PSF), measures 1.0 and 5.0 μm , respectively, for 488-nm excitation and 1.0 and 5.4 μm , respectively, for 543-nm excitation. The chromatic aberration between 488- and 543-nm laser beams is well suppressed. We perform Ca^{2+} imaging in cardiomyocytes through the right ventricular chamber of a perfused rat heart in line-scan mode with 2.9-ms time resolution. We also carried out two-color imaging of a fixed mouse heart and liver with subcellular resolution. The compact head of the microscope equipped with a line-scan imaging mode and two-color imaging mode is useful for *in situ* imaging in living organs with subcellular resolution and can advantageously be applied to *in vivo* research. © 2005 Society of Photo-Optical Instrumentation Engineers. [DOI: 10.1117/1.1890411]

Keywords: compact scanning head; laser scanning microscopy; *in situ* fluorescence imaging; Ca^{2+} imaging; multicolor imaging.

Paper 04097 received Jun. 9, 2004; revised manuscript received Aug. 9, 2004; accepted for publication Aug. 19, 2004; published online Apr. 4, 2005.

1 Introduction

Laser-scanning confocal fluorescence microscopy has revealed various intra- or intercellular functions, such as Ca^{2+} dynamics, with subcellular spatial resolution.^{1,2} Features such as high-speed time-lapse imaging and multicolor imaging are indispensable for elucidating the biological phenomena not only in cultured cells but also in living tissues. Recently, we have established an *in situ* imaging system for monitoring Ca^{2+} concentration ($[\text{Ca}^{2+}]_i$) in rat hearts^{2,3} and have found a variety of abnormal $[\text{Ca}^{2+}]_i$ dynamics within the cardiomyocytes on the epicardial surface under normal rhythm. However, it is difficult to image the endocardial surface of the heart *in situ*, because the chamber of the heart is inaccessible to the bulky microscope. Therefore, a compact and flexible microscope with subcellular resolution is needed for *in situ* or *in vivo* fluorescence imaging of living organs.

For flexibility, fiber optics was introduced for delivery of excitation light and the optical signals from the specimen between an objective lens and the bulk optics part of the microscope, since the optical fiber works as a point light source⁴ as well as a confocal detector.⁵ Since then, several types of compact heads with a single optical fiber⁶⁻⁹ or an optical fiber bundle¹⁰⁻¹³ were developed. The resolution of the single-fiber

scheme is known to be superior to that of the fiber bundle, because the fiber bundle limits the lateral resolution due to the limited number of image points, irregular fiber packing, and coupling of the illumination in the neighboring fibers (cross talk).¹² The head of the single-fiber scheme is, however, larger than one of the fiber bundles relaying the image at the distal end, because the fiber bundle does not require a mechanical scanner in the head. No compact heads have afforded high-speed imaging with millisecond time resolution and multicolor imaging, although resolutions of 1 μm have been attained with the single-fiber scheme⁶⁻⁸ and of 3 μm ^{11,12} with a fiber bundle scheme. Imaging with subcellular resolution in living organs has not been achieved with the compact heads either.

2 Methods and Materials

2.1 Compact Scanning Head

In this research, we employed the single-fiber scheme for 1- μm spatial resolution and a unimorph-scanner-incorporated compact head⁶ for implementing high-speed line scan and multicolor imaging. The apparatus that we have constructed is shown in Fig. 1(a). The compact head used to approach the site of interest has a cylindrical metal cover sleeve with 3.5 mm diam and 30 mm length, and is attached to a metal box containing an optical fiber. The head is small enough to access

Address all correspondence to Tetsuro Takamatsu, Pathology and Cell Regulation, Kyoto Prefectural University of Medicine, Kamigyo-ku, Kyoto 602-8566 Japan; Tel: +8175-251-5322; Fax: +8175-251-5353; E-mail: ttakam@koto.kpu-m.ac.jp

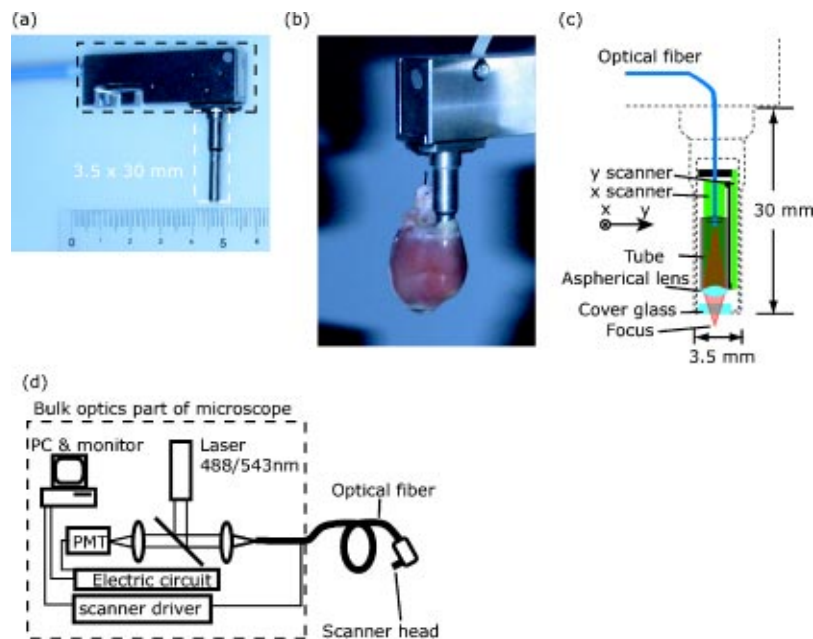


Fig. 1 A compact scanning head for laser confocal fluorescence microscopy. (a) The compact scanning head is outlined by a white dashed box. It measures 3.5 mm in diameter and 30 mm in length. The compact head is attached to a metal box (shown outlined in black) that contains the optical fiber. Although the box is larger than the head, the size can be reduced or the box will be removed for *in vivo* applications in the future. (b) The head can access the ventricular chamber of a Langendorff-perfused living heart. We cut a small area of the right atrium and inserted the head into the heart suspended from a perfusion tube. (c) Schematic cross section of the head showing the aspherical objective lens and two unimorphs operating as an *xy* scanner. Each unimorph moves the tube holding the lens and the end of the optical fiber in one direction. The excitation beam emanates from the tip of the fiber and is focused by the objective lens. (d) Bulk optics of the microscope, shown in the dashed box, supplies the excitation light (Ar^+ laser at 488 nm or He-Ne laser at 543 nm) to the compact head through the optical fiber. The fluorescent signal in the specimen is also delivered through the fiber to the bulk optics.

the right ventricular chamber of the rat heart through an atrium [Fig. 1(b)]. The schematic cross section of the head shows the main components [Fig. 1(c)]. An aspherical objective lens ($\text{NA}=0.55$) and two piezoelectric unimorphs operating together as an *xy* scanner are incorporated inside the metal cover sleeve, and these are packed with a cover glass at the tip of the sleeve, for use under water-immersion conditions. The unimorph moves a tube holding the objective lens and the tip of the fiber, and operates at a resonance frequency of 350 Hz. Consequently, the time resolution in line-scan imaging mode is 2.9 ms. The head is connected to the bulk optics part of the microscope via the optical fiber [Fig. 1(d)]. The typical view field is $90 \times 150 \mu\text{m}$ with a frame rate of 2 Hz.

2.2 Bulk Optics of the Microscope

The microscope is equipped with an Ar^+ laser at 488-nm wavelength and a He-Ne laser at 543-nm wavelength for excitation of fluorescence. These laser beams are coupled with a dichroic mirror. The beam to excite the fluorescence is delivered through an optical fiber with $8.3\text{-}\mu\text{m}$ core (SMF-28, Corning Incorporated). The end of the fiber works as both a point light source and a pinhole for the confocal system. The fluorescent light in the specimen is collected by the objective lens onto the end of the fiber and is delivered through the optical fiber. Then the signal is detected with a photomultiplier tube after proper filtering for cutting unwanted light,

such as reflectance and scattering of excitation laser or the fluorescent signals from other dyes when multifluorescence staining is used.

2.3 Langendorff-Perfused Rat Heart

The heart was excised from a male Wistar rat (9 weeks old) under anesthesia with pentobarbitone sodium according to the Langendorff model at a pressure of 100-cm H_2O for 5 min through the aorta. The perfusion was conducted at 20°C with a HEPES-buffered Tyrode's solution composed of (in mM) NaCl, 140; KCl, 4.0; MgCl_2 , 1.0; CaCl_2 , 1.0; HEPES, 20; and glucose, 10 (pH=7.4 adjusted with NaOH) under oxygenation with 100% O_2 . After washout of the blood for 10 min, the heart was perfused with (Ca^{2+} -free) Tyrode's solution containing a fluorescent Ca^{2+} indicator, Fluo-3/AM, at relatively lower temperatures (19 to 21°C for 45 min). The Fluo-3/AM loading was followed by perfusion with 0.5-mM Ca^{2+} Tyrode's solution at 35 to 37°C for deesterification of the intracellularly loaded Fluo-3/AM (for 10 min). During the experiment, the heart was perfused with Tyrode's solution containing cytochalasin D of $50\text{-}\mu\text{M}$ concentration (033-17563, Wako).

2.4 Immunostaining of the Heart and Liver

The heart and liver were excised from a mouse (B6;129-Gja, wild type) under anaesthesia with pentobarbitone sodium injected intraperitoneally. After washout of the blood with phosphate buffer solution (PBS), the heart and the liver were fixed

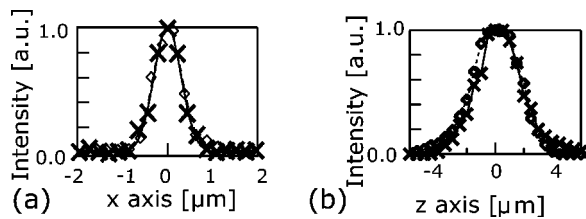


Fig. 2 Lateral and axial PSF. (a) Fluorescence intensity distributions from 100-nm beads. The intensities excited by 488-nm (\times) and 543-nm (\diamond) laser are shown. The intensities are fitted with a Gaussian curve (solid line for 488-nm excitation and dashed line for 543-nm excitation). (b) Response of the reflection from a mirror located around the focal plane. The symbols for 488-nm and 543-nm laser excitation (\times and \diamond) are identical to those shown in (a). The intensities are fitted with a Gaussian curve (solid line for 488 nm and dashed line for 543 nm). The beads for 488-nm and 543-nm excitation were from Polysciences, Incorporated, Warrington, PA, USA (16662) and Duke Scientific Company, Palo Alto, CA, USA (AR100), respectively.

with 4.0% paraformaldehyde for 2 h, followed by permeabilization with 0.5% Triton X-100 for 30 min. Thereafter, the organs were incubated in Alexa Fluor 488 phalloidin (A12379, Molecular Probes, Tokyo, Japan. Incorporated) for 2 h and in propidium iodide (P5264, Sigma Chemical Company, Tokyo, Japan) for another 30 min. To specify the nuclear staining with propidium iodide, the organs were equilibrated in 2X saline-sodium citrate (SSC; NaCl, 0.3 M; sodium citrate, 0.03 M, pH 7.0) for 1 min, incubated in 100- μ g/mL DNase-free RNase in 2X SSC for the following 20 min at 37 $^{\circ}$ C, and rinsed with 2X SSC. During experiments, the heart and liver were immersed in PBS.

3 Results and Discussions

3.1 Spatial Resolution

Since the whole imaging system with the tube at the tip of the fiber is moved for the focus scanning, the optical axis of the beam emerging from the optical fiber is always kept on the axis of the objective lens, even during scanning. We therefore need to concern ourselves only with on-axis aberrations, namely spherical and chromatic aberration, to focus the laser beams tightly with the same focal length as well as to collect the fluorescent light at the specimen to the pinhole detector of the fiber effectively. The aspherical lens has a small amount of wavefront aberration (0.017, 0.011, and 0.005 waves at wavelengths of 488, 543, and 656 nm, respectively, expressed as root mean squares). Figure 2(a) shows the lateral PSF of the microscope, measured as the fluorescence intensity distributions of single 100-nm fluorescent beads placed on a glass substrate. (\times) and (\diamond) show the PSFs obtained with the excitations by the 488- and 543-nm laser beam, respectively. From the full width at half maximum (FWHM) of the PSF, the lateral resolutions are determined to be 1.0 μ m for both 488- and 543-nm excitation. Figure 2(b) shows axial PSFs, measured as the response of the reflection from the mirror moving along the optical axis. From the FWHM, the axial resolutions for 488- and 543-nm beams are determined to be 5.0 and 5.4 μ m, respectively. By use of the aspherical lens, the axial resolution is improved to a greater extent than the lateral resolution compared to the use of a hemispherical lens.⁶ The chromatic aberration is compensated by the cover

glass at the tip of the head, since the cover glass is made of a high-dispersive material, while the objective lens is made of a low-dispersive material. Figure 2(b) shows that there is about 0.5- μ m difference of the focal position (the location of the reflection peak) between the 488- and 543-nm laser beams. This is coincident with the numerical analysis, based on a ray tracing method, predicting that the cover glass suppresses 7 μ m of the focal position difference to 0.52 μ m. We utilized the glass plate in place of a concave lens, which is generally used for chromatic compensation, because of practical considerations involved in assembling the miniaturized components. It is, however, shown that the glass plate composed of high-dispersive material located in the focusing beam is still effective for the chromatic compensation. The working distance of the compact head, defined as the distance from the cover glass to the focus, is about 200 μ m.

3.2 Ca^{2+} Imaging in Cardiomyocytes of a Perfused Rat Heart

The compact head can access the apex of the right ventricular chamber of a Langendorff-perfused rat heart [Fig. 1(b)]. We visualized changes of calcium concentration ($[\text{Ca}^{2+}]_i$) in the subendocardial myocytes with the fluorescent Ca^{2+} indicator Fluo-3. The fluorescence intensities from the cardiomyocytes provided detailed information about the spatial aspects of Ca^{2+} dynamics in the myocytes. In a representative set of the

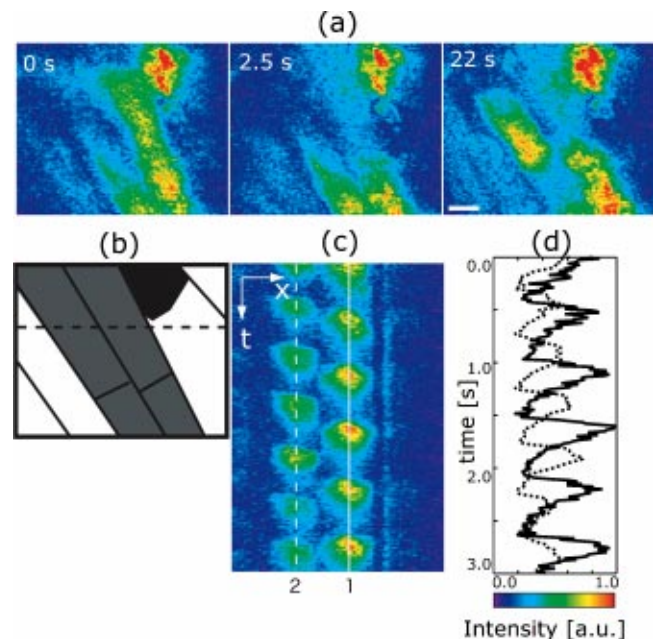


Fig. 3 *In situ* images of $[\text{Ca}^{2+}]_i$ in cardiomyocytes. (a) Three sequential xy images of $[\text{Ca}^{2+}]_i$ detected in cardiomyocytes at the same position. Under attenuation of the mechanical motion of the heart with cytochalasin D, a fixed region of interest was irradiated with an excitation laser (488 nm). The scale bar denotes 10 μ m. (b) Schematic cell shapes and locations. The $[\text{Ca}^{2+}]_i$ fluctuates in four cells (illustrated in gray) and remains at a constant high level in the black cell. (c) A line-scan (x - t) image. The area corresponding to the dashed line in the schematic (b) is imaged with 2.9-ms time resolution. The abscissa denotes the position of the scanning line, and the ordinate, the temporal axis. (d) The line plots of the $[\text{Ca}^{2+}]_i$ changes along the solid line (1) and the dashed line (2) in (c).

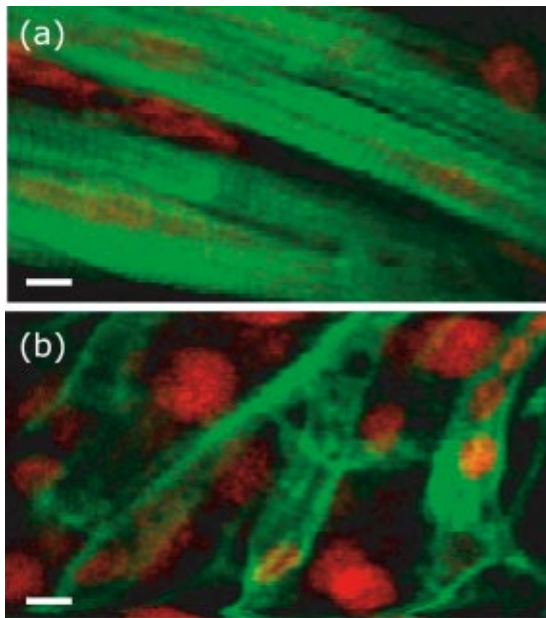


Fig. 4 Two-color images of fixed organs. Actin filaments stained with Alexa Fluor 488 and nuclei stained with propidium iodide are shown. The scale bar denotes 10 μm . (a) A mouse heart. (b) A mouse liver.

sequential xy images of $[\text{Ca}^{2+}]_i$ detected at the same position [Fig. 3(a)], three different images revealed localized fluctuations of $[\text{Ca}^{2+}]_i$, which enabled us to recognize the shapes of the myocytes [Fig. 3(b)]. However, such fluctuations may not reflect the precise behaviors of the myocytes, because the image acquisition time (0.5 s) was too slow to acquire the $[\text{Ca}^{2+}]_i$ dynamics, such as Ca^{2+} transients and Ca^{2+} waves, on a millisecond time scale.^{2,3} To detect the $[\text{Ca}^{2+}]_i$ dynamics with higher time resolution, we imaged myocytes with the line-scan mode that allows shorter time resolution of 2.9 ms. The line-scan image scanned along the dashed line shown in Fig. 3(b) revealed that the $[\text{Ca}^{2+}]_i$ fluctuated in two cardiomyocytes periodically and asynchronously to each other [Fig. 3(c)]. The corresponding line plots [indicated by the dashed line in Fig. 3(d)] clearly demonstrated that these two cells fluctuate at frequencies of 1.8 and 2.1 Hz.

3.3 Two-Color Imaging of Fixed Organs

Two-color imaging provided precise depiction of subcellular structures within the whole fixed organs. As shown in Fig. 4(a), in the myocytes on the subepicardial surface of a mouse heart, the actin filaments and nuclei were clearly visualized by immunostaining with Alexa Fluor 488 phalloidin and propidium iodide, respectively. The cross striations were finely aligned at almost regular intervals of around 2.6 μm . The nuclei in the cells were clearly distinguished from the cytosol. The cell structure and nuclei of the hepatocytes on the surface of the liver were also visualized [Fig. 4(b)]. These observations confirm that the two-color imaging provides a high spa-

tial resolution for subcellular structures in the organs. Though the images are sliced or sectioned with 5.0 or 5.4 μm thickness, we cannot obtain consecutive sectioning images in depth because of the lack of scanning system in depth. These images were obtained with a frame rate of 2 Hz.

4 Conclusion

We successfully develop a compact scanning head for confocal laser microscopy with lateral resolution of 1.0 μm that affords high-speed line-scan imaging and multicolor imaging. The head is small enough for imaging the living heart. This compact microscope system should potentially be a powerful tool not only for basic biological research but also for medical applications, such as *in vivo* diagnosis with endoscopic usage.¹⁴

Acknowledgment

We thank Yoshiharu Saito for fruitful discussion.

References

1. D. J. Stephens and V. J. Allan, "Light microscopy techniques for live cell imaging," *Science* **300**, 82–86 (2003).
2. T. Kaneko, H. Tanaka, M. Oyamada, S. Kawata, and T. Takamatsu, "Three distinct types of Ca^{2+} waves in Langendorff-perfused rat heart revealed by real-time confocal microscopy," *Circ. Res.* **86**, 1093–1099 (2000).
3. K. Fujita and T. Takamatsu, "Real-time in situ calcium imaging with single- and two-photon confocal microscopy," Chap. 23 in *Confocal and Two-Photon Microscopy Foundations, Applications, and Advances*, A. Diaspro, Ed., pp. 483–498, Wiley-Liss, Inc., New York (2002).
4. T. Dabbs and M. Glass, "Fiber-optic confocal microscope: FOCOM," *Appl. Opt.* **31**, 3030–3035 (1992).
5. S. Kimura and T. Wilson, "Confocal scanning optical microscope using single-mode fiber for signal detection," *Appl. Opt.* **30**, 2143–2150 (1991).
6. L. Giniūnas, R. Juškaitis, and S. V. Shatalin, "Scanning fiber-optic microscope," *Electron. Lett.* **27**, 724–726 (1991).
7. P. M. Delaney, M. R. Harris, and R. G. King, "Fiber-optic laser scanning confocal microscope suitable for fluorescence imaging," *Appl. Opt.* **33**, 573–577 (1994).
8. D. L. Dickensheets and G. S. Kino, "Micromachined scanning confocal optical microscope," *Opt. Lett.* **21**, 764–766 (1996).
9. K. Murakami, A. Murata, T. Suga, H. Kitagawa, Y. Kamiya, M. Kubo, K. Matsumoto, H. Miyajima, and M. Katashiro, "A miniature confocal optical microscope with MEMS gimbal scanner," *Proc. IEEE Transducers '03*, pp. 587–590 (2003).
10. A. F. Gmitro and D. Aziz, "Confocal microscopy through a fiber-optic imaging bundle," *Opt. Lett.* **18**, 565–567 (1993).
11. Y. S. Sabharwal, A. R. Rouse, L. Donaldson, M. F. Hopkins, and A. F. Gmitro, "Slit scanning confocal microendoscope for high-resolution *in vivo* imaging," *Appl. Opt.* **38**, 7133–7144 (1999).
12. J. Knittel, L. Schnieder, G. Buess, B. Messerschmidt, and T. Possner, "Endoscope-compatible confocal microscope using a gradient index lens system," *Opt. Commun.* **188**, 267–273 (2001).
13. C. Liang, K. Sung, R. R. Richards-Kortum, and M. R. Descour, "Design of a high-numerical aperture miniature microscope objective for an endoscopic fiber confocal microscope," *Appl. Opt.* **41**, 4603–4610 (2002).
14. M. Sakashita, H. Inoue, H. Kashida, J. I. Tanaka, J. Y. Cho, H. Sato-date, E. Hidaka, T. Yoshida, N. Fukami, Y. Tamegai, A. Shiokawa, and S. E. Kudo, "Virtual histology of colorectal lesions using laser-scanning confocal microscopy," *Endoscopy* **35**, 1–6 (2003).